

# Tunneling Spectroscopy in Superconducting Circuit Lattices

Botao Du,<sup>\*</sup> Qihao Guo, Santiago López, and Ruichao Ma<sup>†</sup>

*Department of Physics and Astronomy, Purdue University, West Lafayette, IN 47907, USA*

(Dated: November 12, 2024)

We demonstrate tunneling spectroscopy of synthetic quantum matter in superconducting circuit lattices. We measure site-resolved excitation spectra by coupling the lattice to engineered driven-dissipative particle baths that serve as local tunneling probes. Using incoherent particle source and drain, we independently extract quasi-particle and quasi-hole spectra and reconstruct the spatial structure of collective excitations. We perform spectroscopy of a strongly interacting Bose-Hubbard lattice at different densities, observing changes in energy gaps across the superfluid to Mott-insulator transition and the effects of three-body interactions. Our results provide a new toolset for characterizing many-body states in analog quantum simulators.

## I. INTRODUCTION

Scanning tunneling spectroscopy has become an essential tool for investigating the electronic properties of quantum materials at the atomic scale [1]. By varying the energy of the probe relative to the sample, tunneling spectroscopy facilitates the extraction of the local density of states for both electrons and holes, thereby providing critical insights into collective excitations in the material and their underlying interactions and correlations. Such local spectroscopy measurements are pivotal for the investigation of superconductivity [2], quantum magnetism [3], and emergent topological states [4].

With recent progress in quantum simulation, engineered quantum systems serve to emulate condensed matter models and study synthetic quantum matter with tunable control and precise readout. Ideas for realizing tunneling spectroscopy in such analog quantum simulators have been proposed for ultracold atoms [5–7], and injection spectroscopy has been recently demonstrated in a non-interacting synthetic lattice [8]. In superconducting circuit quantum simulators, arrays of superconducting resonators and qubits host synthetic quantum matter comprised of interacting microwave photons [9]. Direct microwave spectroscopy measurements can be used to extract lattice parameters [10], measure topological edge states [11], or probe energy-resolved transport [12, 13]. Using coherent local control, the many-body energy spectra can also be extracted from the time-evolution of initial product states [14] or via many-body Ramsey experiments [15]. Nevertheless, it remains a challenge to perform site-resolved spectroscopy in strongly correlated lattices at the level of single collective excitations. Furthermore, the asymmetry between the quasi-particle and quasi-hole spectra provides essential insights into the underlying interactions of the constituent particles. However, most spectroscopic methods in synthetic quantum matter cannot distinguish particle excitations from hole excitations. k, we demonstrate tunneling spectroscopy in

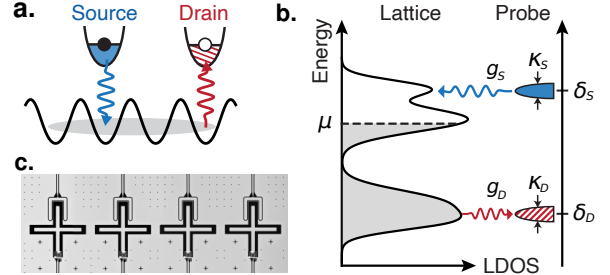


FIG. 1. Illustration of site-resolved tunneling spectroscopy. (a) Locally coupled tunable particle baths act as tunneling probes. (b) The narrow energy bandwidth particle source (particle drain) measures the local density of states of unoccupied quasi-particle (quasi-hole) states. The many-body system is filled to an effective chemical potential  $\mu$ . (c) Image of the superconducting circuit lattice used in this work.

a superconducting circuit lattice by coupling the lattice to engineered driven-dissipative probes. The local probes serve as particle source and particle drain, as realized in our recent work [16], enabling particles to be injected or removed locally with controlled energy. We measure site-resolved particle- and hole- spectra of a strongly interacting Bose-Hubbard lattice, and reconstruct the spatial structure of quasi-particles from the site-resolved spectra. By performing the spectroscopy at different lattice fillings, we reveal changes in the excitation gap across the superfluid to Mott insulator transitions and directly observe the effects of multi-particle interaction. These experiments provide a new toolset for manipulating and characterizing quantum many-body states in superconducting circuits.

## II. LOCAL LATTICE EXCITATION SPECTRA

Consider a tight-binding lattice model that hosts an interacting many-body state, illustrated in Fig. 1. We perform tunneling spectroscopy by coupling lattice sites to particle baths with tunable narrow-band energy, and extract the local excitation spectra of the many-body state from the tunneling current between the lattice site and

<sup>\*</sup> du245@purdue.edu

<sup>†</sup> maruichao@purdue.edu

the probe as their energy detuning is varied. If the lattice is a closed system apart from its coupling to the probe, we can infer the tunneling current via the change in the total particle number in the lattice. Here, we will employ two types of particle baths as the tunneling probe to access both the quasi-particle and quasi-hole spectra: If the probe is a particle source ( $S$ ), particles are added to the many-body state at the energies of unoccupied quasi-particle states. If the probe is a particle drain ( $D$ ), particles are removed from the many-body state at energies that match the unoccupied quasi-hole states.

For a many-body state  $\psi_0$  with energy  $E_0$ , the local quasi-particle [quasi-hole] excitation spectrum at lattice site  $x$  as a function of the probe frequency  $\omega$  is:

$$I_x^{\text{part[hole]}}(\omega) = \sum_s |\langle \phi_s | a_x^\dagger [a_x] | \psi_0 \rangle|^2 \delta\left(\frac{E_s - E_0}{\hbar} - \omega\right) \quad (1)$$

$a_x^\dagger (a_x)$  is the particle creation (annihilation) operator on lattice site  $x$ , and the sum in  $s$  is over all many-body eigenstates of the lattice with eigenenergy  $E_s$  and eigenfunction  $\phi_s$ . In real systems, the frequency  $\delta$ -function will have finite widths given by the intrinsic decoherence.

When site  $x$  is coupled to a local particle source (drain), the rate of increase (decrease) of the total particle number  $N$  in the lattice is given by the quasi-particle (quasi-hole) spectra  $I_x(\omega)$  convoluted with a time-dependent frequency kernel  $K$  [6]:

$$\begin{aligned} \frac{d}{dt} \langle N(t, \omega, x) \rangle &= \frac{4g_S^2}{\kappa_S} \int d\omega' I_x^{\text{part}}(\omega') K(\omega - \omega', t) \\ \frac{d}{dt} \langle N(t, \omega, x) \rangle &= -\frac{4g_D^2}{\kappa_D} \int d\omega' I_x^{\text{hole}}(\omega') K(\omega - \omega', t) \end{aligned} \quad (2)$$

Here  $g_S$  ( $g_D$ ) is the effective tunnel-coupling between the lattice site and the particle source (drain), and  $\hbar$  is the reduced Planck constant.  $\langle N(t, \omega, x) \rangle$  is the expectation value of the total particle number in the lattice after the tunneling probe with center frequency  $\omega$  has been coupled to site  $x$  for a duration of  $t$ . The effective frequency resolution, captured in  $K$ , is jointly determined by the frequency bandwidth of the probes ( $\kappa_{D/S}$ ), the effective coupling between the lattice and the probes ( $g_{D/S}$ ), and the Fourier-limited bandwidth from the finite probing time ( $\delta\omega \sim 2\pi/t$ ). We use  $\delta_{D/S}$  to denote the detuning between the probe frequency and the lattice frequency.

### III. SPECTROSCOPY OF A CIRCUIT BOSE-HUBBARD LATTICE

We demonstrate tunneling spectroscopy in a strongly interacting superconducting circuit Bose-Hubbard lattice comprised of a one-dimensional array of four transmon qubits where the particles are microwave photons (Fig. 1c, see detailed device parameters and experimental

setup in [16]). The lattice is described by the Hamiltonian:

$$\begin{aligned} \mathcal{H}_{\text{BH}}/\hbar &= \sum_{\langle ij \rangle} J a_i^\dagger a_j + \frac{U_2}{2} \sum_i n_i(n_i - 1) \\ &+ \frac{U_3}{6} \sum_i n_i(n_i - 1)(n_i - 2) + \sum_i \epsilon_i n_i \end{aligned} \quad (3)$$

Here  $a_i^\dagger$  is the bosonic creation operator for a microwave excitation on lattice site  $i$ ,  $J$  is the nearest neighbor tunneling rate,  $n_i = a_i^\dagger a_i$  is the on-site occupancy,  $U_2$  ( $U_3$ ) is the on-site two-body (three-body) interaction, and  $\epsilon_i$  is the on-site energy. In our device, the effective on-site interactions are given by the energy level structure of the transmon qubit [17], corresponding to  $U_2 \approx -2\pi \times 245$  MHz and  $U_3 \approx -2\pi \times 28$  MHz. Experiments in this work are limited to on-site occupancy  $n_i \leq 3$ , so higher-order interactions beyond three-body are irrelevant. The capacitive coupling between neighboring transmons determines the fixed  $J \approx 2\pi \times 5.9$  MHz. We also have a small residual next-nearest neighbor tunneling  $J_{\text{NNN}} \approx 2\pi \times 0.5$  MHz which we include in the calculated lattice spectra below. The on-site energies  $\epsilon_i$  are tunable within  $2\pi \times (4.0 - 5.7)$  GHz using local flux control lines. Microwave photons in the lattice have a typical relaxation rate of  $\Gamma_1 = 1/T_1 \approx 1/(30 \mu\text{s}) \approx 2\pi \times 5$  kHz measured from single transmon lifetimes, and a local dephasing rate of  $\Gamma_\phi = 1/T_2^* \approx 1/(2.5 \mu\text{s}) \approx 2\pi \times 60$  kHz.

As demonstrated in our previous work [16], we create local tunable particle baths in a hardware-efficient way by inducing resonant coupling between the transmon lattice sites and their individual readout resonators. Parametric modulation of the transmon frequency at the sum (difference) of the transmon and resonator frequencies creates an effective incoherent particle source (drain). The strength and frequency of the modulation determines the tunable coupling strength  $g_{D/S}$  and frequency detuning  $\delta_{D/S}$ . For experiments in this work, we keep  $g_{D/S}$  small compared to the resonator linewidth  $\kappa_r \approx 2\pi \times 1.5$  MHz. In this weak coupling limit, the incoherent particle baths represent tunneling probes that are effectively non-interacting and infinite; the baths have spectral width  $\kappa_{D/S}$  equal to the resonator linewidth  $\kappa_r$ , which sets the frequency resolution for the tunneling spectroscopy.

In the limit  $g_{D/S} \ll \kappa_{D/S} \ll J$ , relevant for experiments in this work, the change in the total particle number  $\Delta N(t) = N(t) - N(0)$  as a function of the probe duration  $t$  can be qualitatively understood as follows (see similar discussions in Ref. [6]): (i) At very short times when the Fourier limited spectral width of the probe is wide enough to cover many resonances ( $2\pi/t \gg J$ , or  $t \ll 2\pi/J \approx 150$  ns), the total population change  $\Delta N$  resembles that of Fermi's golden rule and scales linearly with time ( $\Delta N \propto t$ ). (ii) Shortly after, the Fourier limited spectral width becomes smaller than the energy resolution set by the probe linewidth  $\kappa$  ( $t \geq 2\pi/\kappa_r \approx 670$  ns), and the probe could resolve individual many-body tran-

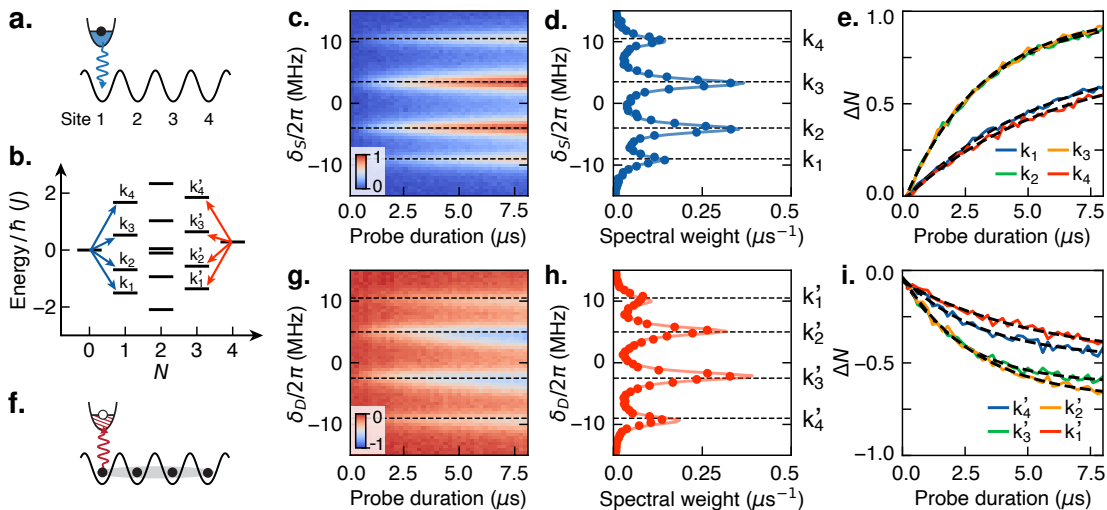


FIG. 2. Measuring local excitation spectra of a Bose-Hubbard lattice. (a) Tunnel-coupled particle source probes quasi-particle excitations of the empty lattice, illustrated in the many-body spectrum (b). (c) Measured population change as a function of probe detuning and duration  $\Delta N(\delta_S, t)$ , and (e) data and exponential fits at the four resonant detunings  $\delta_S$ . (d) The measured (dots) and numerically calculated (line) quasi-particle spectrum. (f) Tunnel-coupled particle drain probes quasi-hole excitations of the  $n = 1$  Mott state. (g) Measured probe-induced population change  $\Delta N(\delta_D, t)$ , and (i) data and exponential fits at the four resonant  $\delta_D$ . (h) The measured and calculated quasi-hole spectrum. Data in all figures are typically averaged over 10,000 experimental runs, with standard errors of the mean below 1%. Other systematic uncertainties in the measured population are below  $\pm 1\%$ , see [16].

sitions if  $\kappa_r \ll J$ . When the probe is on resonance with a particular transition, the population change is quadratic in time according to time-dependent perturbation theory ( $\Delta N \propto t^2$ ). As we will see later, for parameters used in this paper, the early time dynamics described in (i-ii) only correspond to a small change in the lattice population  $\Delta N \ll 1$ . (iii) As the population change increases, the dynamics of  $\Delta N$  are affected by the change in the many-body state. Due to the strong on-site interaction  $U_2$ , the many-body excitation spectrum also exhibits large nonlinearities. When the nonlinearity is larger than the probe's energy resolution, the particle source (drain) will only be able to add (remove) one excitation from the many-body state and become off-resonant with the energy of the second excitation. In this limit, the population change in the lattice saturates towards  $\Delta N \approx 1$  ( $-1$ ) with a time constant given by  $\kappa_r / (4g_{S(D)}^2 I_x(\omega))$ . The spectral weight  $I_x(\omega)$  reflects the corresponding excitation's transition matrix element; the prefactor can be derived from Eq. 2 or following Fermi's golden rule.

### A. Quasi-particle and quasi-hole spectra

We start by measuring the particle excitation spectrum of an initially empty lattice with all sites at the same frequency  $\omega_{\text{latt}} \approx 2\pi \times 4.6$  GHz (Fig. 2a). We couple the first lattice site to its local particle source with a coupling rate  $g_S \approx 2\pi \times 0.25$  MHz and measure the total population after a variable probe duration of up to  $t = 8 \mu\text{s}$ . The individual readout resonators allow us to

perform multiplexed readout of the on-site occupancy. In Fig. 2c, we plot  $\Delta N(t)$  measured at different probe detuning  $\delta_S$ . We observe population growth at four distinct detunings, corresponding to the resonant population transfer from the particle bath into the four single-particle eigenstates of the lattice, labeled as  $k_1$  to  $k_4$ . The single-particle states correspond to quasi-momentum eigenstates of the lattice with an energy dispersion of  $\sim \pm 2J$ . These processes are illustrated in the many-body spectrum (Fig. 1b), here showing only states in the hard-core boson limit with on-site occupancy  $n_i \leq 1$ . On resonance with each transition,  $\Delta N$  saturates towards 1. Here, the rate for the resonant probe to put a second particle into the lattice is about two orders of magnitude smaller than the single-particle excitation rates, as a result of the frequency mismatch in the non-linear spectrum and the wavefunction overlap.

To obtain the particle excitation spectra, we fit  $\Delta N(t)$  at each detuning to an exponential function and extract the relative spectral weight from the slope of the fitted exponential at  $t = 0$ . For the probe parameters here, the initial dynamics during which  $\Delta N$  changes non-exponentially only contribute a small  $\Delta N \ll 1$  so the exponentials fit well to the measured data as seen in Fig. 2e. From the fits at the four resonant frequencies,  $\Delta N$  saturates to values very close to 1 at  $k_2$  and  $k_3$ . For  $k_1$  and  $k_4$ , the fitted  $\Delta N$  saturates towards  $\approx 0.8$ , due to the competition between the relatively weak pumping rate from the particle bath and the intrinsic relaxation in the lattice. In general, if the spectrum has (near-) degenerate multi-particle excitations,  $\Delta N$  may not saturate towards

1 or follow a well-defined exponential at longer times. However, our analysis method can still yield an accurate spectrum if the exponential fit is applied only to data from early times when  $\Delta N < 1$ . The measured particle spectrum of the vacuum state is shown in Fig. 2d, in excellent agreement with the spectrum calculated from Eq. 1-2 without any free parameters. For the calculation, we use a Lorentzian with linewidth  $\kappa_r$  and unity amplitude as the frequency kernel  $K$ , and the eigenstates and eigenenergies are obtained from  $\mathcal{H}_{\text{BH}}$  using the measured lattice parameters. While we measure and show the full dynamics of  $\Delta N(t)$  here, only a few different probe durations are needed to extract the spectra accurately.

Next, we show the measurement of the quasi-hole spectrum. We choose the  $n = 1$  Mott insulator with one particle per lattice site as the initial state. In the Mott state, on-site particle number fluctuations are highly suppressed by the strong interaction  $U_2$ . The  $n = 1$  Mott state is prepared by applying individual resonant  $\pi$  pulses on each transmon lattice site while they are detuned, then using the fast flux controls to rapidly move them to  $\omega_{\text{latt}}$ . We couple the first site to the local particle drain to perform the tunneling spectroscopy (Fig. 2f). Similar to the particle source above, the particle drain has an energy resolution given by the resonator linewidth  $\kappa_r$  and we use a coupling strength of  $g_D \approx 2\pi \times 0.25$  MHz.

For an initial state with finite population and probe duration up to  $8\mu\text{s}$ , the intrinsic relaxation in the lattice leads to population decay even when the probe is off-resonant from any transitions. We separately measure the intrinsic decay  $N_0(t)$  with the probe off and subtract it from the measured  $N(t)$  with the probe on to obtain the probe-induced population change  $\Delta N(t) = N(t) - N_0(t)$ , plotted in Fig. 2g as a function of the probe detuning  $\delta_S$ . In the hard-core limit, the Bose-Hubbard model exhibits particle-hole symmetry. The quasi-hole excitations appear at probe detunings that are reversed from the frequencies of the quasi-hole states in the many-body spectra, as seen in Fig. 2h. This is because a quasi-hole state with negative detuning is occupied by a particle with positive detuning during the tunneling spectroscopy. In our case, the single-particle/hole dispersions are slightly asymmetric as a result of the finite  $J_{\text{NNN}}$  and the negative finite  $U_2$ . In Fig. 2i, we show the population change at each of the four quasi-hole resonances. The drain-induced population change saturates towards  $\Delta N \sim -0.6$  for  $k'_2$  and  $k'_3$  and  $\Delta N \sim -0.45$  for  $k'_1$  and  $k'_4$ . These smaller  $|\Delta N|$ , compared to the expected value of 1, result from the intrinsic lattice relaxation. Without coupling to any probe, the transmon  $T_1$  would lead to a population decay of  $\Delta N_0 \approx -1$  in a duration of  $8\mu\text{s}$  starting from the Mott state. Since the probe is only resonantly coupled to one transition in the non-linear many-body spectrum, the drain-induced population change becomes suppressed as the initial Mott

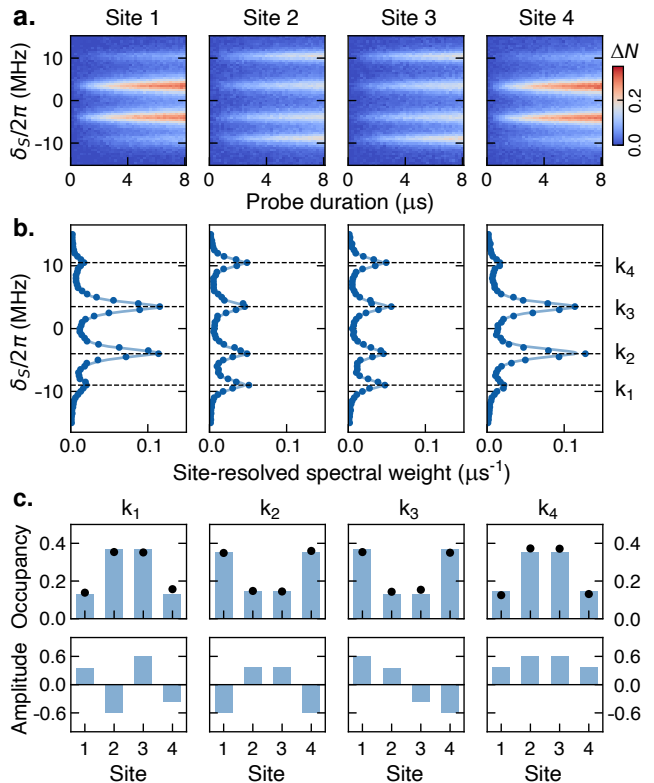


FIG. 3. Reconstruct single-particle wavefunctions using site-resolved spectra. (a) Population change on each lattice site for the experiment in Fig. 2a-e. (b) Measured spectra from data in (a). Lines are fit to a sum of Lorentzians with width  $\kappa_r$  to obtain the site-resolved spectral weights for each single-particle mode  $k_1$  to  $k_4$ . (c) On-site occupancy of the single-particle eigenstates from the normalized spectral weights. Dots are data, and bars are from calculated eigenstates. (d) Calculated on-site amplitudes of the corresponding wavefunctions.

state decays.

In general, the intrinsic relaxation of many-body states is a complex cascaded state-dependent process. However, our measurement is robust to weak decoherence because we extract the spectral weights from the fitted slopes at early times when the population change due to intrinsic relaxation is small. We observe good agreement between the measured quasi-hole spectrum of the  $n = 1$  Mott state and the calculation (Fig. 2h). The measured spectrum has a slightly lower amplitude than the calculated spectra, with an overall scaling of  $\approx 90\%$ . We attribute this to state preparation errors that result in a reduced initial population in the  $n = 1$  Mott state.

## B. Imaging quasi-particle wavefunctions

In addition to the spectral information, the site-resolved readout in our circuit Bose-Hubbard lattice also provides spatial information of the quasi-particle and quasi-hole excitations. As a simple demonstration, we

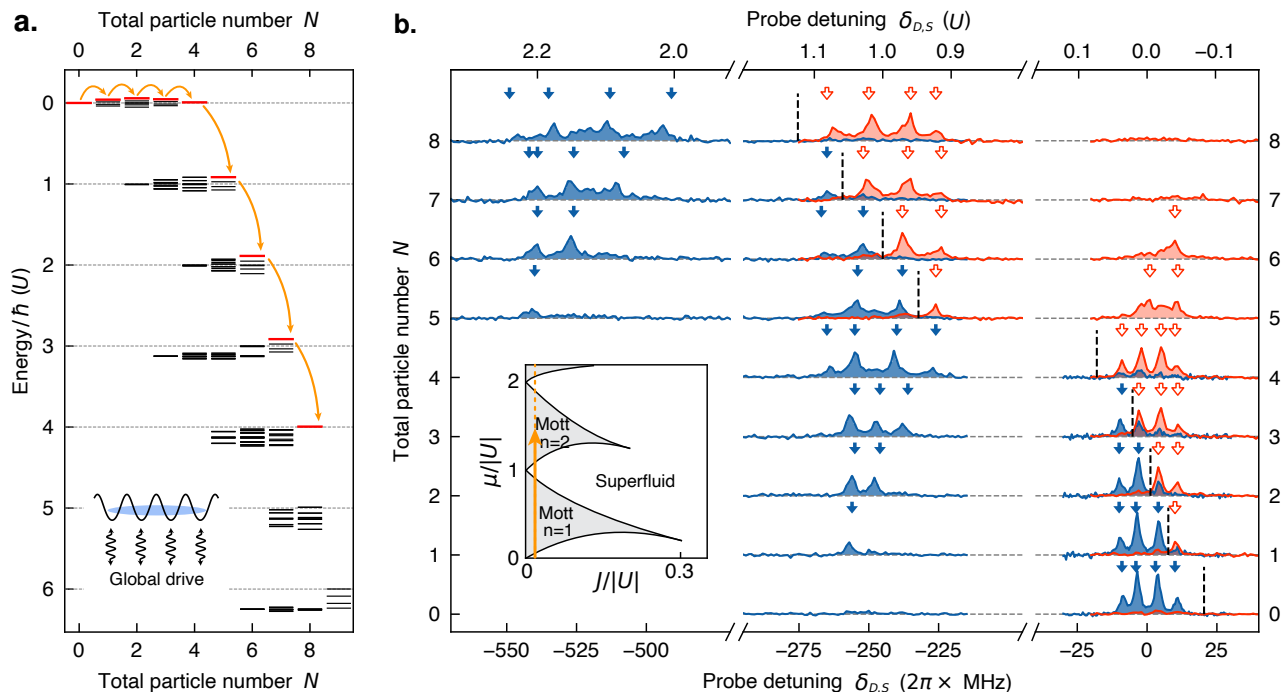


FIG. 4. Density-dependent tunneling spectroscopy. (a) Many-body spectra of the Bose-Hubbard lattice beyond the hard-core limit. We prepare the highest-energy states for  $N$  up to 8 (red thick lines) with a time-varying global coherent drive (inset) that sequentially populates the lattice via many-body Landau-Zener transitions (orange arrows). (b) The measured quasi-particle spectra (blue with dark fill) and quasi-hole spectra (red with light fill) at each lattice population  $N$ , probed at site 1. The dotted vertical lines indicate the end detuning of the coherent drive used to prepare each state, which acts as the effective chemical potential  $\mu$ . Arrows above the spectra show frequencies of calculated excitations. The inset in (b) illustrates the phase diagram, and the vertical arrow indicates the states we accessed. The regions behind the insets contain no spectral features.

measure the on-site occupancy of single-particle eigenstates using the same tunneling spectroscopy experiment described in Fig. 2a-e. In Fig. 3a, we plot the particle number change on each lattice site during the tunneling spectroscopy. We use the same exponential fitting methods discussed previously to obtain the site-resolved quasi-particle spectra shown in Fig. 3b. We fit the spectra with sums of Lorentzians with fixed linewidth  $\kappa_j$ ; the amplitudes of the Lorentzians give the spectral weight at each site  $i$  and for each eigenstate  $k_j$ . For each of the four single-particle eigenstates, the site-resolved spectral weights are directly proportional to the on-site occupancies of the wavefunction. In Fig. 3c, we show the normalized on-site occupancies for the four single-particle quasi-momentum eigenstates, in agreement with the calculated densities from the single-particle wavefunctions.

Here, we used the site-resolved readout with a spatially fixed local probe to obtain the spatial density distributions of collective excitations in the lattice. Alternatively, we can perform tunneling spectroscopy with the probe coupled to different lattice sites and measure the spatial distribution from the local spectral weights. Our hardware-efficient implementation of the tunneling probe is well suited for such analogous scanning tunneling spectroscopy. Beyond simple single-particle states, the tunneling probe needs sufficient energy resolution to excite

and measure a single collective excitation in a generic many-body state. Hence the method demonstrated here can be applied to gapped phases or finite-size systems with large non-linearities to reveal spatial information of collective excitations.

### C. Spectroscopy across the superfluid to Mott insulator transition

We now perform the tunneling spectroscopy at different filling densities of the Bose-Hubbard lattice. As the many-body state undergoes density-induced transitions between strongly correlated superfluids and Mott insulators, we use the measured excitation spectra to identify changes in the energy gap in different quantum phases and observe the effects of multi-particle interactions.

We use a global coherent microwave drive to adiabatically populate the lattice via many-body Landau Zener transitions [16], illustrated in Fig. 4a. Starting with an empty lattice, we turn on the global drive at frequency  $\omega_{\text{drive}}$  to a Rabi rate of  $\Omega_{\text{drive}} = 2\pi \times 4.0$  MHz in 300 ns with an initial detuning  $\omega_{\text{drive}} - \omega_{\text{latt}} = 2\pi \times 30$  MHz  $\approx 5J$ . We then sweep  $\omega_{\text{drive}}$  at a rate of  $-2\pi \times 80$  MHz/ $\mu$ s to different end drive frequencies  $\omega_{\text{drive}}^{\text{end}}$ , before turning off the drive in 300 ns. Using drive sweeps with end de-

tunings  $\omega_{\text{drive}}^{\text{end}} - \omega_{\text{latt}} = 2\pi \times \{7.6, 1.2, -5.2, -18\}$  MHz  $\approx \{1.2J, 0.2J, -0.9J, -3J\}$ , we prepare the highest energy eigenstates with total particle number  $N = \{1, 2, 3, 4\}$  respectively. The  $N = 4$  state is the  $n = 1$  Mott insulator. Here, the end drive detuning acts as an effective chemical potential  $\mu$  that determines the total particle number in the lattice. Starting from the state with  $N = 4$ , we apply a second global coherent drive to prepare states with  $N > 4$  beyond the hard-core boson limit. We start at drive detuning  $-2\pi \times 205$  MHz  $\approx U_2 + 6.7J$  and stop at end detunings of  $2\pi \times \{-232.2, -245, -259.4, -275.4\}$  MHz  $\approx \{U_2 + 2J, U_2, U_2 - 2.4J, U_2 - 5J\}$ , to populate the highest energy eigenstates with  $N = \{5, 6, 7, 8\}$  respectively. The  $N = 8$  state is the doubly-filled  $n = 2$  Mott insulator. States other than  $N = 4$  and 8 are strongly correlated superfluids that exhibit large on-site number fluctuations and interaction-induced density-density correlations [18]. Our transmon lattice has  $U < 0$ , representing a strongly attractive Bose-Hubbard model. By preparing the highest energy states in the finite-size lattice, we effectively study the physics of the ground states of the strongly repulsive Bose-Hubbard model. As  $N$  increases from 0 to 8, we traverse a path in the phase diagram of the 1D Bose-Hubbard model illustrated in the inset of Fig. 4b (see for example the predicted phase diagram in Ref. [19]).

The measured density-dependent quasi-particle and quasi-hole spectra are shown in Fig. 4b. For  $N = 0$ , the particle spectrum has been shown previously in Fig. 2a. The hole spectrum shows small finite amplitudes at the same single-particle eigenstate frequencies; these result from the equilibrium thermal population in the lattice which is measured to be approximately 5% per site. For  $N = 1, 2, 3$ , the superfluid states show low-frequency quasi-hole and quasi-particle excitations in the ground band with probe detunings  $|\delta_{\text{D,S}}| \lesssim 2J$ . The observed asymmetry between the particle and hole spectra is a signature of the strong interactions. In addition, states with  $N \geq 1$  can be excited to states in the second band with two particles on the same site, which appear in the quasi-particle spectra near  $\delta_{\text{S}} \sim U_2$  due to the on-site two-body interaction.

At  $N = 4$  (the  $n = 1$  Mott state), all quasi-hole excitations appear in the ground band while the quasi-particle excitations are separated by  $\sim U_2$  in the second band. This energy separation is the characteristic Mott gap of the insulating Mott phase. The quasi-particle states in the second band contain one delocalized particle tunneling on top of a unity-filled  $n = 1$  Mott state, which tunnels with a bosonic enhanced rate of  $2J$ . As a result, the excitations in the second band have a larger frequency dispersion spanning  $|\delta_{\text{D,S}} - U_2| \lesssim 2 \times 2J$ . The small residual amplitude of the particle excitation peaks in the ground band is from imperfect preparation of the  $n = 1$  Mott state due to thermal population and decoherence during the adiabatic drive.

The states we prepared at  $N = 5, 6, 7$  are once again correlated superfluids, while  $N = 8$  is the  $n = 2$  Mott insulator. Beyond the ground and second band excita-

tions, these states with  $N \geq 5$  can be excited to states in the third band with three particles on the same site. A third particle on a lattice site will experience both the two-body interaction  $U_2$  and three-body interaction  $U_3$ , so these quasi-particle resonances appear near probe detunings  $\delta_{\text{S}} \sim 2U_2 + U_3$ . For example, the quasi-particle excitations of the  $N = 8$  Mott state correspond to a delocalized particle with a bosonic enhanced tunneling rate of  $3J$  on top of the doubly-filled Mott state. As seen in the plotted spectra, these excitations to the third band are observed at probe frequencies in the range of  $|\delta_{\text{S}} - 2U_2 - U_3| \lesssim 3 \times 2J$ . Therefore, our measurements provide a direct spectroscopic probe of the dispersion and interactions of the transmon lattice beyond the hard-core limit. Utilizing higher levels of transmons opens new possibilities for analog quantum simulation [20]. For instance, the realization of lattice models with dominant  $U_3$  interaction using effective cancellation of  $U_2$  [21] could lead to strongly-correlated phases with charge-density-wave order [22].

#### IV. DISCUSSION AND OUTLOOK

The tunneling spectroscopy demonstrated in this paper offers several advantages over existing spectroscopic methods in superconducting circuit lattices. Conventional spectroscopy relies on weak and long coherent drives to achieve high energy resolution, where the absorption/emission signals result from the balance between external drive and intrinsic dissipation. The exact rates of the driving or dissipation are difficult to characterize a priori and generally vary for different many-body states, thereby complicating the extraction of accurate spectral weights. In our method, the tunneling rate is set by the controlled coupling to the incoherent probe, making the obtained spectra insensitive to weak intrinsic decoherence. Moreover, the ability to distinguish between quasi-hole and quasi-particle excitations, as we demonstrated, remains challenging in conventional coherent spectroscopy.

Our locally coupled probes enable site-resolved tunneling spectroscopy that is well-suited for investigating systems with spatially varying excitations. Examples include studying many-body localized systems by measuring the local level statistics and the spatial extent of rare Griffiths regions [23, 24]; and understanding strongly correlated topological models by probing edge states in hard-core Su-Schrieffer-Heeger models [25] or interacting chiral edge states in a Chern insulator [26].

In this paper, we used the multiplexed readout to measure the population across the entire lattice to infer the probe-induced tunneling current. To further reduce the measurement overhead, we can directly measure the tunneling current between the probe and the lattice [16]. Instead of the incoherent particle baths in this work, coherent two-level systems coupled to the lattice could also serve as tunneling probes [6, 27].

Another potential extension is the use of multiple local probes: Employing both a source and a drain would enable energy- and site-resolved pump-probe spectroscopy to provide insights into the non-equilibrium dynamics. The dynamics of collective excitations can be accessed by varying the delay between the bath-induced excitation and a subsequent spectroscopy measurement. Momentum-resolved spectroscopy has also been proposed, where arrays of local probes are coupled to the lattice to extract the spectral function [28].

Finally, our experiments open the door for the dissipative preparation of quantum many-body states using incoherent particle baths [29]. The spectrally narrow baths can be used to populate strongly correlated states sequentially [30], and combining the energy-selective par-

ticle source and drain enables the autonomous stabilization of many-body phases in photonic synthetic quantum matter [31].

## ACKNOWLEDGEMENTS

This work was supported by grants from the National Science Foundation (award number DMR-2145323) and the Air Force Office of Scientific Research (award number FA9550-23-1-0491). Part of this material is based upon work supported by the U.S. Department of Energy, Office of Science, National Quantum Information Science Research Centers, Quantum Science Center.

- 
- [1] C. J. Chen, *Introduction to Scanning Tunneling Microscopy* (Oxford University Press, Oxford, 2007).
- [2] Ø. Fischer, M. Kugler, I. Maggio-Aprile, C. Berthod, and C. Renner, Scanning tunneling spectroscopy of high-temperature superconductors, *Rev. Mod. Phys.* **79**, 353 (2007).
- [3] Z. Qiu, M. Holwill, T. Olsen, P. Lyu, J. Li, H. Fang, H. Yang, M. Kashchenko, K. S. Novoselov, and J. Lu, Visualizing atomic structure and magnetism of 2D magnetic insulators via tunneling through graphene, *Nat. Commun.* **12**, 70 (2021).
- [4] J.-X. Yin, S. H. Pan, and M. Zahid Hasan, Probing topological quantum matter with scanning tunnelling microscopy, *Nat. Rev. Phys.* **3**, 249 (2021).
- [5] C. Kollath, M. Köhl, and T. Giamarchi, Scanning tunneling microscopy for ultracold atoms, *Phys. Rev. A* **76**, 063602 (2007).
- [6] A. Kantian, U. Schollwöck, and T. Giamarchi, Lattice-Assisted spectroscopy: A generalized scanning tunneling microscope for ultracold atoms, *Phys. Rev. Lett.* **115**, 165301 (2015).
- [7] D. Gruss, C.-C. Chien, J. T. Barreiro, M. Di Ventra, and M. Zwolak, An energy-resolved atomic scanning probe, *New J. Phys.* **20**, 115005 (2018).
- [8] S. N. M. Paladugu, T. Chen, F. A. An, B. Yan, and B. Gadway, Injection spectroscopy of momentum state lattices, *Communications Physics* **7**, 1 (2024).
- [9] I. Carusotto, A. A. Houck, A. J. Kollár, P. Roushan, D. I. Schuster, and J. Simon, Photonic materials in circuit quantum electrodynamics, *Nat. Phys.* **16**, 268 (2020).
- [10] R. Ma, C. Owens, A. LaChapelle, D. I. Schuster, and J. Simon, Hamiltonian tomography of photonic lattices, *Phys. Rev. A* **95**, 062120 (2017).
- [11] C. Owens, A. LaChapelle, B. Saxberg, B. M. Anderson, R. Ma, J. Simon, and D. I. Schuster, Quarter-flux hofstadter lattice in a qubit-compatible microwave cavity array, *Phys. Rev. A* **97**, 013818 (2018).
- [12] M. Fitzpatrick, N. M. Sundaresan, A. C. Y. Li, J. Koch, and A. A. Houck, Observation of a dissipative phase transition in a One-Dimensional circuit QED lattice, *Phys. Rev. X* **7**, 011016 (2017).
- [13] G. P. Fedorov, S. V. Remizov, D. S. Shapiro, W. V. Pogosov, E. Egorova, I. Tsitsilin, M. Andronik, A. A. Dobronosova, I. A. Rodionov, O. V. Astafiev, and A. V. Ustinov, Photon transport in a Bose-Hubbard chain of superconducting artificial atoms, *Phys. Rev. Lett.* **126**, 180503 (2021).
- [14] P. Roushan, C. Neill, J. Tangpanitanon, V. M. Bastidas, A. Megrant, R. Barends, Y. Chen, Z. Chen, B. Chiaro, A. Dunsworth, A. Fowler, B. Foxen, M. Giustina, E. Jeffrey, J. Kelly, E. Lucero, J. Mutus, M. Neeley, C. Quintana, D. Sank, A. Vainsencher, J. Wenner, T. White, H. Neven, D. G. Angelakis, and J. Martinis, Spectroscopic signatures of localization with interacting photons in superconducting qubits, *Science* **358**, 1175 (2017).
- [15] G. Roberts, A. Vrajitoarea, B. Saxberg, M. G. Panetta, J. Simon, and D. I. Schuster, Manybody interferometry of quantum fluids, *Science Advances* **10**, eado1069 (2024).
- [16] B. Du, R. Suresh, S. López, J. Cadiente, and R. Ma, Probing site-resolved current in strongly interacting superconducting circuit lattices, *Phys. Rev. Lett.* **133**, 060601 (2024).
- [17] J. Koch, T. M. Yu, J. Gambetta, A. A. Houck, D. I. Schuster, J. Majer, A. Blais, M. H. Devoret, S. M. Girvin, and R. J. Schoelkopf, Charge-insensitive qubit design derived from the cooper pair box, *Phys. Rev. A* **76**, 042319 (2007).
- [18] B. Saxberg, A. Vrajitoarea, G. Roberts, M. G. Panetta, J. Simon, and D. I. Schuster, Disorder-assisted assembly of strongly correlated fluids of light, *Nature* **612**, 435 (2022).
- [19] S. Ejima, H. Fehske, and F. Gebhard, Dynamic properties of the one-dimensional bose-hubbard model, *EPL* **93**, 30002 (2011).
- [20] O. Mansikkamäki, S. Laine, A. Piltonen, and M. Silveri, Beyond hard-core bosons in transmon arrays, *PRX Quantum* **3**, 040314 (2022).
- [21] L. Cardarelli, S. Greschner, and L. Santos, Engineering interactions and anyon statistics by multicolor lattice-depth modulations, *Phys. Rev. A* **94**, 023615 (2016).
- [22] A. J. Daley and J. Simon, Effective three-body interactions via photon-assisted tunneling in an optical lattice, *Phys. Rev. A* **89**, 053619 (2014).
- [23] D. A. Abanin, E. Altman, I. Bloch, and M. Serbyn, Colloquium : Many-body localization, thermalization, and entanglement, *Rev. Mod. Phys.* **91** (2019).

- [24] K. Agarwal, E. Altman, E. Demler, S. Gopalakrishnan, D. A. Huse, and M. Knap, Rare-region effects and dynamics near the many-body localization transition, *Ann. Phys.* **529**, 1600326 (2017).
- [25] S. de Léséleuc, V. Lienhard, P. Scholl, D. Barredo, S. Weber, N. Lang, H. P. Büchler, T. Lahaye, and A. Browaeys, Observation of a symmetry-protected topological phase of interacting bosons with rydberg atoms, *Science* **365**, 775 (2019).
- [26] J. C. Owens, M. G. Panetta, B. Saxberg, G. Roberts, S. Chakram, R. Ma, A. Vrajitoarea, J. Simon, and D. I. Schuster, Chiral cavity quantum electrodynamics, *Nat. Phys.* **18**, 1048 (2022).
- [27] J. P. T. Stenger, G. Ben-Shach, D. Pekker, and N. T. Bronn, Simulating spectroscopy experiments with a superconducting quantum computer, *Phys. Rev. Res.* **4** (2022).
- [28] K. Zawadzki and A. E. Feiguin, Time- and momentum-resolved tunneling spectroscopy of pump-driven nonthermal excitations in mott insulators, *Phys. Rev. B.* **100**, 195124 (2019).
- [29] R. Ma, B. Saxberg, C. Owens, N. Leung, Y. Lu, J. Simon, and D. I. Schuster, A dissipatively stabilized mott insulator of photons, *Nature* **566**, 51 (2019).
- [30] R. O. Umucalılar and I. Carusotto, Generation and spectroscopic signatures of a fractional quantum hall liquid of photons in an incoherently pumped optical cavity, *Phys. Rev. A* **96**, 053808 (2017).
- [31] J. Lebreuilly and I. Carusotto, Quantum simulation of zero-temperature quantum phases and incompressible states of light via non-markovian reservoir engineering techniques, *C. R. Phys.* **19**, 433 (2018).